Performance of a Cylindrical Phase-Change Thermal Energy Storage Unit

R. Ponnappan* and Dean L. Jacobson†
Arizona State University, Tempe, Arizona

An experimental apparatus with a water-circulated calorimeter was designed and constructed to evaluate the high-temperature performance of a phase-change material (PCM) in a cylindrical thermal-energy-storage container (TESC) sample. A 12 in. long, 1 in. diam Inconel 617 container filled with a eutectic PCM of 64 LiF-30MgF_2-6KF salt was tested. The phase-change characteristics of the salt during melting and solidification were observed by monitoring the external axial temperature profile of the container. Energy was supplied to the sample by radiation from a resistance heater and energy was rejected to the calorimeter by radiation. The sample container was mounted in an ion-pumped vacuum chamber. Analysis of phase-change heat transfer in cylindrical geometry was based on the modified heat balance integral method of Tien which provided the solidification rate and time. The thermal diffusivity of the salt at its fusion temperature was then calculated. The experimental results obtained for the eutectic salt melting point (710°C), freezing point (671°C), latent heat of fusion (782 J/g), and thermal diffusivity (0.00799 cm^2/s) were in good agreement with those found in the literature. The experimental and analytical results of the nondimensionalized heat-transfer resistance as a function of the solidified or melted weight fraction were compared.

Nomenclature

A = surface area of thermal energy storage container
C_p = specific heat
G = reciprocal of Stefan number, $L/C_p(T_m - T_c)$
H = Biot number, $\bar{h}_r r_0/k_s$
h = heat-transfer coefficient
$\bar{h}$ = average heat-transfer coefficient
k = thermal conductivity
L = latent heat (enthalpy of fusion)
ℓ = length of the TESC sample
m = mass
$\dot{Q}$ = heat flow rate
R_H = resistance to heat transfer in an annular layer of the phase-change material
R_H^* = dimensionless form of R_H defined in Eq. (8)
r = radial distance
$\bar{r}$ = dimensionless radius, r/r_0
St = Stefan number, $1/G$
T = temperature, °C
$\bar{T}$ = dimensionless temperature, $(T - T_c)/(T_m - T_c)$
t = time
$\bar{t}$ = Fourier number, $\alpha t/r_0^2$
V = volume of the TESC
α = thermal diffusivity
Δt = time interval defined in Eq. (11)
Δt_f = time duration of fusion
ΔT = temperature difference
ϵ = location of the liquid-solid interface
$\bar{\epsilon}$ = dimensionless form of ϵ, ϵ/r_0
ρ = density
χ = weight of the solidified PCM to the total weight

Subscripts

c = cold surroundings
cal = calorimeter
cw = cooling water
f,F = fusion
ℓ = liquid phase
lh = latent heat
m = melting
o = outer
PCM = phase-change material
r = radiative
s = solid phase
W = wall of the TESC

Presented as Paper 82-0076 at the AIAA 20th Aerospace Sciences Meeting, Orlando, Fla., Jan. 11-14, 1982; submitted June 28, 1982; revision received Oct. 7, 1982.

*Graduate Student; presently Thermal Engineer, Universal Energy Systems Inc., Dayton, Ohio. Member AIAA.

†Professor, Mechanical and Aerospace Engineering Department. Member AIAA.

Introduction

THE latent-heat thermal-energy-storage (TES) concept is attractive because of its high-energy storage densities over a narrow temperature range. Promising applications both in space and terrestrial thermal systems[1,2] are apparent. Eutectic mixtures of fluoride salts have been found to release energy on the order of 1.25-4.25 GJ/m^3 in the temperature range of 900-1000 K. The thermophysical properties of such high-temperature phase-change materials (PCM) and the heat-transfer characteristics of TES devices containing them are very important in the design of thermal systems.

The objective of the present work was to design and construct a calorimeter system capable of working in a vacuum in order to evaluate the performance of a given cylindrical TES unit made of Inconel 617 and filled with the eutectic mixture of 64LiF-30MgF_2-6KF salt. This setup was planned to measure the melting and solidification temperatures and the latent heat of fusion of the fluoride salt.

The data obtained provided a means of verifying an analytical model for solidification time and surface temperature. The thermal diffusivity of the PCM at its fusion temperature was calculated from the experimental information.

Theoretical Considerations of Melting and Solidification in a Cylinder

Analytical methods of solving the moving-phase boundary problems range from the general approximate method of London and Seban[3] to the modified heat balance integral (MHBI) method of Tien.[4] Some of the other significant works are the heat balance integral method of Goodman,[5] the generalized numerical method of Tao,[6] and the enthalpy model of Shamsundar and Sparrow.[7] The recent work of Tien on the solidification of cylindrical samples is an appropriate model for the analysis of energy extraction for the present TES system.

Problem Formulation

The problem considered is the freezing of an infinitely long cylinder of molten PCM when the latent-heat extraction takes place at its outer surface with a constant coefficient of radiative heat transfer for the cooling coil of the calorimeter. The coordinate system and the boundary conditions of this problem are set as in Fig. 1.

The following idealizations are made in order to represent the experimental unit with a convenient mathematical model:

1) The ends of the cylindrical thermal-energy-storage container (TESC) are adiabatic.

2) Energy leaving the TESC wall is purely radiative and is completely absorbed by the calorimeter cooling coil.

3) The TESC has uniform emittance, and an average heat-transfer coefficient $\bar{h}_r$ can be obtained from steady-state heat losses.

4) Energy loss through lead wires and mounting fixtures are negligible and can be accounted for experimentally.

5) Thermal capacitive effects of the heater blocks and the TESC wall are negligible.

6) The material (PCM) behaves like a pure substance so that its liquid, solid transition occurs at a single temperature, that is, at the melting point.

7) The liquid is at its melting point just at the start of solidification which means that there is no heat transfer within the liquid.

8) Physical properties (α, C_p, ρ, k) are temperature independent and they are constant for the solid and liquid phases.

9) Convection effects within the liquid are negligible.

10) No supercooling occurs upon solidification.

Under these assumptions, the temperature distribution within the solid and the propagation rate of the liquid, solid interface (or freezing rate) are obtained from the one-dimensional heat-conduction equation in cylindrical coordinates given by the normalized partial differential equation together with the initial and boundary conditions as follows.

Partial differential equation,

$$\frac{1}{\bar{r}}\frac{\partial}{\partial \bar{r}}\bar{r}\frac{\partial \bar{T}}{\partial \bar{r}} = \frac{\partial \bar{T}}{\partial \bar{t}} \tag{1}$$

$$\bar{T} = 1 \quad \text{at} \quad \bar{r} = \bar{\epsilon} \tag{2}$$

Boundary condition,

$$\frac{\partial \bar{T}}{\partial \bar{r}} = G\frac{d\bar{\epsilon}}{d\bar{t}} \quad \text{at} \quad \bar{r} = \bar{\epsilon} \tag{3}$$

$$\frac{\partial \bar{T}}{\partial \bar{r}} = -H\bar{T} \quad \text{at} \quad \bar{r} = 1 \tag{4}$$

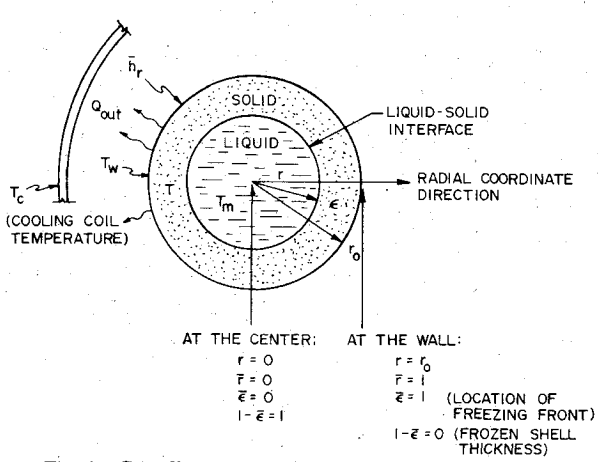

Fig. 1 Coordinate system for the cylindrical geometry.

Initial condition,

$$\bar{\epsilon} = 1 \quad \text{at} \quad \bar{t} = 0 \tag{5}$$

where the normalized parameters are defined as,

$$\bar{T} = \frac{T - T_c}{T_m - T_c}; \quad \bar{r} = \frac{r}{r_0}; \quad \bar{t} = \frac{\epsilon}{r_0}; \quad \bar{\epsilon} = \frac{\alpha t}{r_0^2} \quad \text{(Fourier number)}$$

$$H = \frac{\bar{h}_r \cdot r_0}{k_s} \quad \text{(Biot number)}$$

$$G = \frac{L}{C_p(T_m - T_c)} \quad \text{(Reciprocal Stefan number)}$$

Integration of Eq. (1) with respect to $\bar{r}$ between $\bar{r} = \bar{\epsilon}$ and $\bar{r} = 1$ and using the boundary conditions gives,

$$\frac{d\theta}{d\bar{t}} = -(1+G)\bar{\epsilon}\frac{d\bar{\epsilon}}{d\bar{t}} - H\bar{T}|_{\bar{r}=1} \tag{6}$$

where

$$\theta = \int_{\bar{\epsilon}}^{1} \bar{r}\bar{T}\,d\bar{r}$$

Equation (6) is the integral form of the heat-conduction equation which has to be solved for the temperature $\bar{T}$ and freezing front $\bar{\epsilon}$ by suitable techniques.

Solution of the Heat Balance Integral

The MHBI method of Tien[4] has been used to transform Eq. (6) into a second-order ordinary-differential equation with two initial conditions by assuming a quadratic function as the solution for $\bar{T}[\bar{\epsilon}(\bar{t}), \bar{r}]$. The initial-value problem obtained has been solved numerically by using the fourth or fifth-order Runge-Kutta method with an IBM-AMDAHL 360 computer system. A computer program was written and used in conjunction with a CAN program called SUBROUTINE RKF45. The results of this computation are shown later in Figs. 10 and 11 and discussed in the results and analysis section along with the experimental results.

Heat-Transfer Resistance

As soon as the solidification process begins, an interface of the solid and liquid PCM is created which moves away from the original heat exchange surface. The layer of solid PCM bounded by the wall and the interface offers a resistance which is a function of time, geometry, and material. This resistance for the annular layer of the solid PCM shown in Fig. 1 can be written as

$$R_H = \frac{\ell n r_0/\epsilon}{2\pi k_s} \tag{7}$$

This is nondimensionalized by multiplying R_H by the factor $k_s A^2/V$ where A is the area of heat exchange and V the volume of the PCM. Hence the theoretical normalized

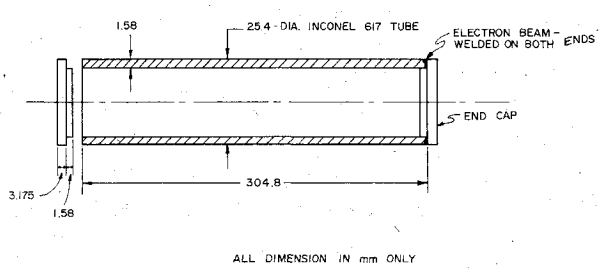

Fig. 2 TESC sample.

resistance R_H^* is obtained as

$$R_H^* = R_H \frac{k_s A^2}{V} = -2\ell n(\bar{\epsilon}) \tag{8}$$

which is a function of the location of the freezing front. R_H^* varies from zero at the start of the solidification ($\bar{\epsilon}=1$) to infinity toward the end ($\bar{\epsilon}=0$), and this provides the theoretical bound for an ideal cylindrical TES system.

The quantity $\bar{\epsilon}$ in Eq. (8) can be expressed in terms of a fraction χ defined as

$$\chi = \frac{\text{weight of the annular layer solidified}}{\text{weight of the total PCM}}$$

or

$$\chi = (r_0^2 - \epsilon^2)/r_0^2 = 1 - \bar{\epsilon}^2 \tag{9}$$

Therefore Eq. (8) can be expressed in terms of χ as

$$R_H^* = -\ell n\,(1-\chi) \tag{10}$$

Further, in terms of energy extraction from the PCM, the fraction χ can be expressed as a time-dependent function as

$$\chi(t) = \frac{1}{\dot{m}_{\text{PCM}} L} \int_0^t \dot{Q}_{lh}(t)\,\Delta t \tag{11}$$

where the integrand represents the latent-heat release from the start of solidification up to any instant of time t within the region of "temperature arrest." Figure 9 compares the theoretical and experimental resistance values.

Performance of a Cylindrical TESC

Physical Details of the Sample

The TESC sample is 12 in. long and 1 in. in diameter (o.d.) and its cross section is shown in Fig. 2. The container has a longitudinal seam-welded body and electron-beam-welded flat end caps, all made of Inconel 617. It has been filled under extreme cleanliness conditions with 225.519 g of the eutectic fluoride salt and the total weight is 571.2 g. The container design and filling details are given in Ref. 8.

Description of the Experimental Setup

The setup consists of a vacuum chamber 8 in. in diameter (i.d.), which is a cross-shaped stainless steel tubular chamber fitted with detachable vacuum-joint flanges and feed-throughs and hooked to a Vacsorb, Vacion pumping unit of 40 l/s capacity, and a calorimeter which includes the TESC sample, electric heater blocks of the clamshell type in two cylindrical halves, Chromel-Alumel thermocouple temperature-measuring circuitry and instrumentation, and a water-circulated copper cooling coil. A schematic diagram of the experimental setup is given in Fig. 3.

The calorimeter was designed to minimize heat losses and to maintain a uniform temperature throughout the length of the TESC and had an electric heater of the semicylindrical annular-shell type. Together with the thermocouples the TESC was housed inside the core region of the heater shells, and this whole assembly was held concentrically inside a closely coiled copper water-cooling coil which in turn was inside the vacuum chamber. The water line and electrical and thermocouple lead connections were taken out through proper feed-throughs in the vacuum chamber. The cooling coil was insulated with stainless-steel and aluminum foils to prevent radiation loss to the outer wall. Convection loss was eliminated by evacuating the chamber to at least 10^{-3} Torr. The only mode of heat exchange allowed between the TESC and heater assembly and the cooling coil was by radiation. Figure 4 gives the schematic diagram of the calorimeter.

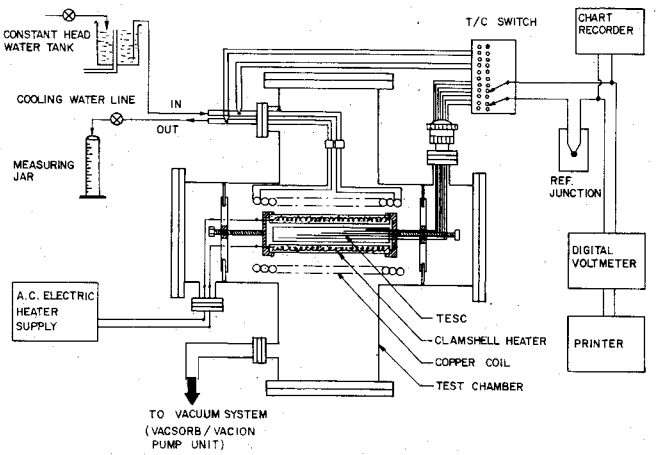

Fig. 3 Schematic experimental setup.

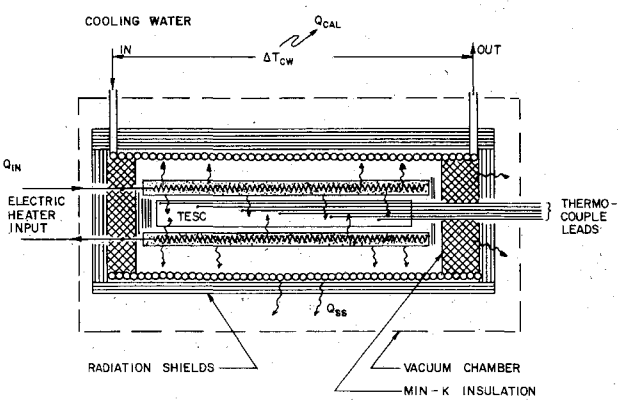

Fig. 4 Schematic calorimeter.

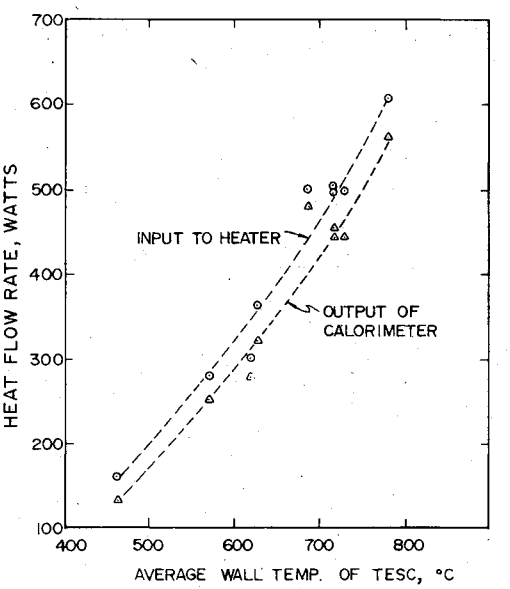

Fig. 5 Steady-state heat loss.

The energy required to heat the TESC to the salt melting point (that is from ambient to 710°C) was estimated to be 242.8 W·h assuming no heat losses. A heat loss equal to that from the outer surface of the electric heater during a 45 min heating period produces a calculated power of 650 W.

The water-cooling coil design was based on the criteria of maximum energy input to the TESC and minimum temperature differential between the inlet and outlet water temperatures. Maximum output occurred when the TESC was maintained at steady state above the melting point of the salt (998 K). A maximum temperature rise to 363 K was assumed

in order to avoid boiling the water within the coil. With these values the radiated power absorbed by the cooling coil was 905 W and the cooling water flow rate required was 22 l/h, A constant-head water tank arrangement provided a maximum flow rate of 40 l/h, which was adequate for the present experiment. The cooling coil was formed out of annealed 3/8 in. copper tube with 37 closely coiled helical turns with a 3.5 in. coil i.d. Three to four layers of polished stainless-steel sheet wrapped around the cooling coil provided the thermal insulation at the periphery while MIN-K-type high-temperature insulation together with two to three layers of aluminum foil shielded the ends.

A vacuum environment was necessary for this experiment in order to avoid oxidation of the TESC wall when heated to high temperatures and to make the heat-balance calculations simpler by eliminating convection heat losses from the TESC. However, conduction loss through the thermocouple and electric heater lead wires and through the mounting fixtures were not fully eliminated but minimized. The vacuum system was a Varian Vacsorb, Vacion pumping unit which provided 10^{-6} Torr.

Experimental Procedure

Electrical power to the heater was supplied through a variac and watt meter and the input could be regulated. The power input reading on the watt-meter was counterchecked by precisely measuring the resistance of the heater coil in steady-state conditions (998 K) and the voltage input. Energy output through the circulating water was obtained by monitoring the inlet and outlet temperatures and the flow rate.

Temperatures along the length of TESC outer wall were measured with nine 20 SWG Chromel-Alumel thermocouples. Thin ceramic beads for high-temperature application were used to give rigidity and insulation for the thermocouples. Proper contact of the thermocouple bead with the TESC wall was insured by a strap of stainless-steel strip spot welded around the TESC. The thermocouples were connected to the instrumentation consisting of a junction box, a switch, a thermoelectric reference junction, a digital voltmeter, and a printer. A continuous chart recording of the TESC wall temperature at a slow speed of 1 in./h indicated whether or not steady state was attained.

Experimental Results and Analysis

Steady-State Losses and Temperature Profiles

Steady-state heat losses for the system were calculated by measuring the heater input and the calorimeter output powers when the temperatures of all the thermocouples remained steady. The difference between the input and output powers gave the steady-state losses which account for the heat lost by conduction in thermocouple leads, heater electrical leads, and the TESC support pivots and by radiation at the ends where no cooling coils were present. These measurements were made at different power input levels of 150 to 600 W. Tests were repeated several times with inputs sufficient to cause melting such that repeatability was insured. Figure 5 shows the steady-state losses as a function of TESC wall average temperature. The losses vary from 25 W at 723 K to 50 W at 1023 K which is about 8 to 16% of the input power. Surface temperatures along the axial lengths of the TESC were monitored at different conditions of the cooling cycle. Figure 6 provides the representative axial temperature profiles of the horizontal-axis test. The profiles indicate that the temperature remained fairly uniform at the center section while the end temperatures dropped below the average. The large gradient was due to the uncontrollable end and lead losses of the system.

Melting and Freezing Points of the Salt

The melting point of the salt could not be directly measured since the salt was in a sealed container. Temperature measurements on the container wall during heating of the

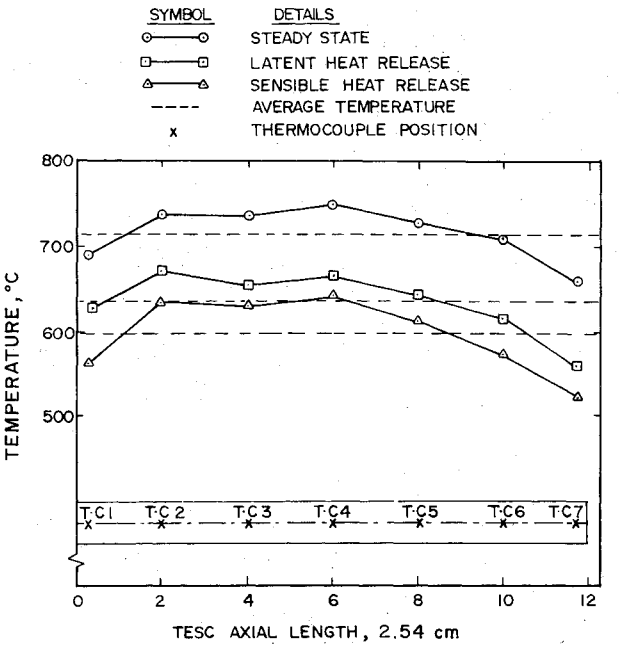

Fig. 6 Axial temperature profile.

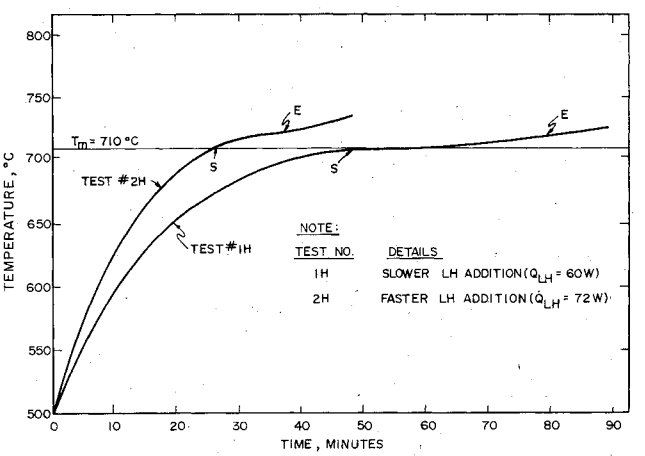

Fig. 7 Melting curves.

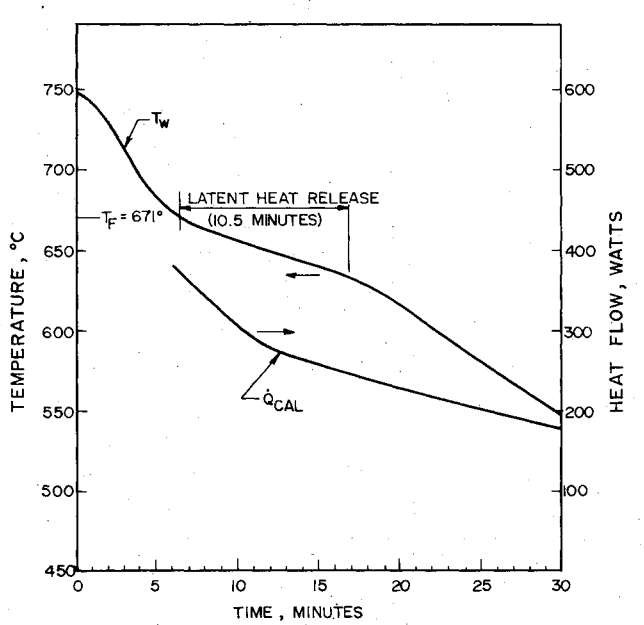

Fig. 8 Solidification curve (test 2C).

TESC provided an indirect method of obtaining the melting point. The melting curves for two different heating conditions are plotted in Fig. 7 and it can be seen that the latent heat addition takes place at fairly constant temperatures near 983 ±2 K which corresponds to the melting point. This agrees very well with the results of 986 and of 983 K reported in Refs. 9 and 10, respectively. An error of ±5 K is reasonable in this value in order to account for the measurement errors, the temperature drop across the TESC wall, and the nonuniformity in the axial temperature of the unit.

Solidification Temperature

The freezing point may not be the same as the melting point. Differences arise because of subcooling and the effects of impurities. Melting points are generally reproducible but often freezing points are not. Figure 8 is a typical solidification curve. The freezing point is approximately the constant-temperature region in which the latent-heat release takes place. Due to the external temperature measurement and the loss of sensible heat from the solidified shell, the constant temperature region does not appear exactly constant. As soon

Table 1 Thermophysical properties of the salt (PCM)

Serial No.	Details		Data source Ref.
1	Salt	$LiF\text{-}MgF_2\text{-}KF$ eutectic mixture	
2	Composition, %	63.5-30.5-6 (molar)	9, 13
3	Density, g/cm^3		
	Solid at 25°C	2.918	
	Liquid at 750°C	2.182 ±0.022	13
4	Conductivity, at		
	fusion temp, W/cm·°C	0.0711	11
5	Specific heat, J/g·°C		
	Solid at fusion temp	2.025	9
	Computed from other data	3.638	13
6	Diffusivity, cm^2/s		
	Solid at 25°C	0.017	13
	Solid at 455°C	0.009	—[a]
	Solid at fusion temp	0.00799	
	Computed $\alpha = k/\rho C_p$	0.00896	11, 13
7	Latent heat of fusion, J/g		
	By DTA method	753.6	13
	By DSC method	793.5	9
	Method not known	814.12	11
	Present experiment	782.26	—[a]
8	Thermal events, K		
		Melting point / Freezing point	
	By DSC method	986 / 955	9
	By DTA method	981 / 976	13
	Method unknown	983 / —	11
	Present experiment	983 / 944	—[a]

[a] Results of the present experiment.

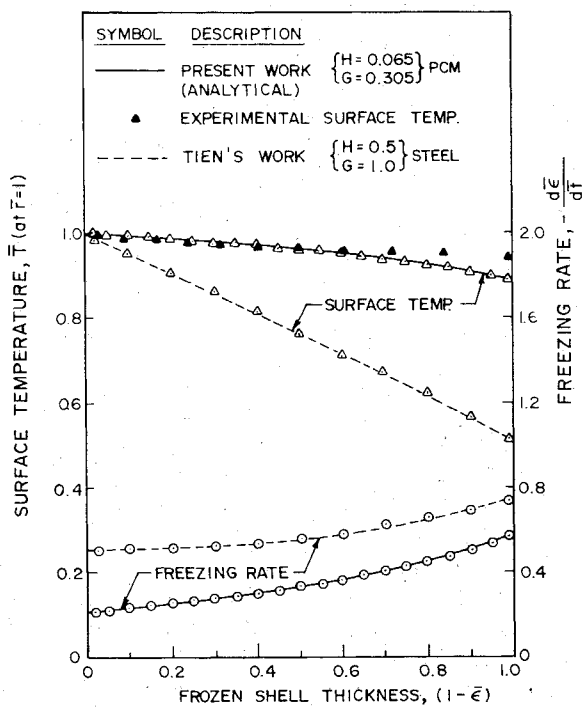

Fig. 9 Heat-transfer resistance of PCM during solidification and/or melting.

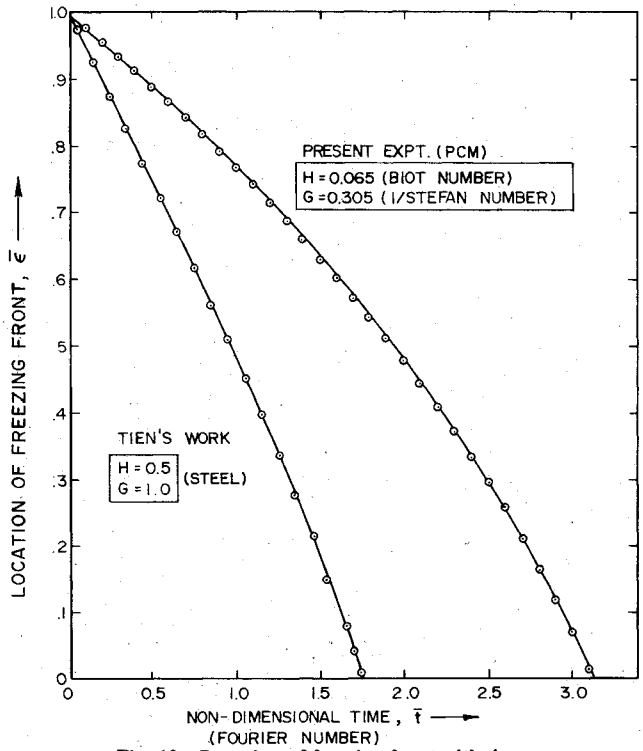

Fig. 10 Location of freezing front with time.

as the solidification begins, a shell of solid PCM forms at the inside of the TESC wall around the core of the molten PCM. When the solidification proceeds with time, the TESC wall temperature cools down even though the molten-core temperature remains constant at the melting point. In the present experiment it was observed that the solidification started when the wall temperature was approximately 944 K and this value was reproducible during all of the solidification tests (about 23 tests). The solidification temperature for the same eutectic mixture measured by a direct method[9] (differential scanning calorimetry by Perkin-Elmer Corporation) has been reported as 955 K and by an indirect method[10] similar to the present experiment as 978 K.

Latent Heat and Solidification Time

In the present experiment it was observed that the latent-heat release took place over a temperature range of 25 K and the duration of "temperature arrest" was about 10.5 min as shown in Fig. 8. The latent-heat release was estimated by the simple energy-balance relation,

$$\dot{Q}_{\text{out}} \Delta t_f = \dot{m}_{\text{PCM}} L \tag{12}$$

or $L = \dot{Q}_{\text{out}} \Delta t_f / m_{\text{PCM}}$ which yields $L = 782.26$ J/g.

This value closely agrees with 793.50 J/g reported in Ref. 9. Table 1 compares the results of the present experiment with those from the literature.

Heat-Transfer Parameters

The TESC and the cooling coil are radiatively coupled since the test chamber was evacuated to 10^{-5} Torr or better. When the capacitive effects of the heater shell on the heat transfer between the TESC and the cooling coil were neglected the overall heat-transfer coefficient due to radiation was evaluated as

$$h_r = \frac{\dot{Q}_{\text{cal}}}{A(\bar{T}_w - \bar{T}_{cw})} \tag{13}$$

For the present setup, h_r varied from 31 to 42 W/m$^2 \cdot$°C for $\dot{Q}_{\text{cal}}$ between 562 and 44 W. $\bar{T}_w$ varied between 1052 and 735. K while $\bar{T}_{cw} = 303$ K and $A = 0.024322$ m^2.

The dimensionless parameter representing the ratio of the internal to the external resistance of the TESC defined using the radius of the cylindrical TES as the significant dimension is the Biot number and this was calculated as $H \simeq 0.065$ using the available literature value for k_s. The Stefan number which gives the ratio of the heat of fusion to the sensible heat between the fusion point and the sink temperature was computed as $St \simeq 3.27$ or $G \simeq 0.305$. This number represents a property of the PCM, and PCMs generally have St values between 0 and 4 as noted in Ref. 12. The Fourier number representing the nondimensionalized time required to solidify a given thickness of salt was the basis for estimating the thermal diffusibility of the salt.

Comparison of Experimental and Theoretical Results

The nondimensionalized resistance to heat transfer R_H^* and the solidified or melted fraction of the PCM, χ are plotted (R_H^* as a function of χ) in Fig. 9. In this figure the resistance curves obtained for the melting and solidification processes at different heat flow rates are compared with the theoretical resistance for the cylindrical geometry. The resistance curves for solidification follow the theory somewhat closely and tend to merge only at the end of complete solidification. The reason for the deviation may be attributed to possible nonuniform freezing within the cylinder, as is evident from the axial temperature profiles shown in Fig. 6. The uneven start of solidification directly violates the assumption of concentric solidification and hence results in larger resistance values in actual experiments. For the same solidified fraction χ higher heat flow has lower resistance since the heat transfer occurs at nearly the same temperature difference.

The resistance curves for melting differ from the theoretical curve. This is due to the assumption of equal thermal conductivity for the solid and liquid phases ($k_s = k_\ell$) which in practice is not true. There are no other published data for k_ℓ for this salt. Using the estimated value of k_ℓ, a correction could be applied in computing R_H^* for the melting cases as shown in Fig. 9. This correction brings the curves to that of the solidification cases. For the same χ higher heat flow has a larger resistance contrary to the freezing case. This could be due to incomplete and nonuniform melting. If the thermal conductivity of the molten salt is accurately known, the resistance values of melting and freezing in a cylinder under identical heat flow can be estimated correctly. The resistance curves could assist in understanding the TESC behavior with respect to a given geometry and in general this would help to determine proper size and shape.

The analysis for obtaining the location of the solid, liquid interface in the solidification process in a cylinder has been examined earlier and the result of the analysis for the present experimental parameters ($H = 0.065$, $G = 0.305$) is shown in Fig. 10 and are compared with the results of Tien[4] for $H = 0.5$ and $G = 1.0$. It was determined that the computer program performed as projected in Ref. 4 and the computations were repeated for the H and G values obtained here. It can be seen that the location of the freezing front or the solid, liquid interface depends on the H and G values, while the initial slope of the curve at the start of solidification is determined from $d\bar{\epsilon}/d\bar{t} = -(H/G)$ which is linear and constant for the given H and G. As demonstrated by Tien, this computation accurately produces the time at which the freezing front would reach the center without encountering the problems faced by some of the earlier semianalytical works.[5,6] Since the solidification depends upon G (a physical property of the TES) and H (a parameter of the operating system) it is very easy to compute the freezing front and the time of complete solidification for any H and G.

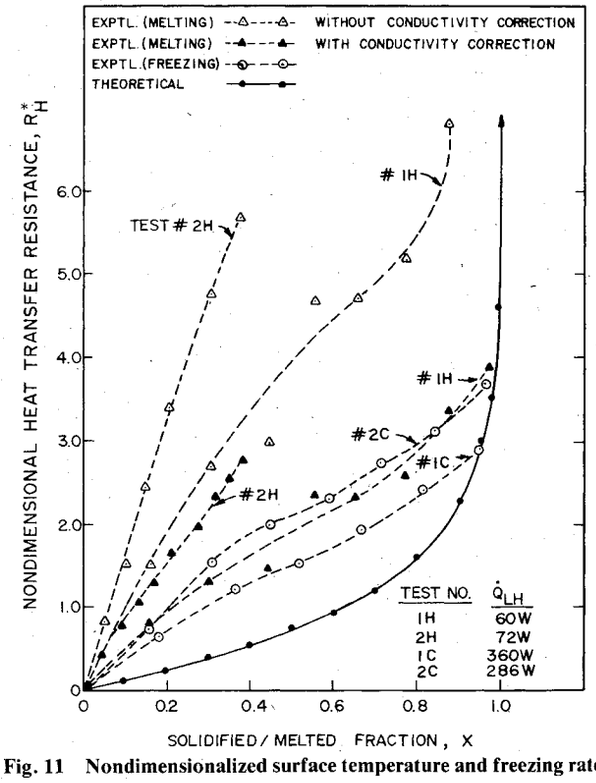

Fig. 11 Nondimensionalized surface temperature and freezing rate.

Surface Temperature and Freezing Rate

The computer program also allowed computation of the nondimensional surface temperature $\bar{T}$ and freezing rate $-d\bar{\epsilon}/d\bar{t}$ of the TES material as a function of frozen shell thickness $(1-\bar{\epsilon})$. The curves obtained for the present experiment are shown compared with those of Tien in Fig. 11. In order to compare the numerically computed surface temperatures with the experimentally measured values the cooling curve temperatures corresponding to the "temperature-arrest" region were plotted after normalizing in Fig. 11. Since there was no possibility of experimentally measuring the frozen-shell thickness $(1-\bar{\epsilon})$, the abscissa for the experimental $\bar{T}$ was taken as the theoretical value corresponding to $\bar{t}$ from Fig. 10. The experimental surface temperature tends to drop more slowly than that of the analytical prediction toward the end of complete solidification. This deviation could be attributed to the unaccounted thermal mass of the TESC metal wall and the heater blocks present in the system.

Thermal Diffusivity of TES Salt

The thermal diffusivity α of the TES material was obtained from the relation $\alpha = r_0^2 \bar{t}/t$. Substituting the values obtained from Fig. 10 as $\bar{t} = 3.12$ for complete solidification and from Fig. 8 as $t = 10.5$ min, α for the 2.54 cm diam TESC is determined to be 0.00799 cm^2/s. This value corresponds to the fusion temperature of 944 K and it lies close to the value $\alpha_{728\,K} = 0.009\ cm^2/s$ reported in Ref. 13.

Conclusions

In the present work a calorimeter system capable of working in a vacuum was designed and assembled to evaluate the heating and cooling characteristics of a cylindrical thermal energy storage container filled with a eutectic mixture of 64LiF-30MgF_2-6KF salt. Thermal data of the salt namely, melting freezing points, latent heat of fusion, and diffusivity were determined from the experimental data. The results were a melting temperature of 983 K, a freezing temperature of 944 K, a latent heat of fusion of 782.26 J/g, and a thermal diffusivity at the fusion temperature of 0.00799 cm^2/s. The results corroborated with values in the literature. Thermal diffusivity value at the fusion temperature by direct measurement was not available.

The modified heat-balance-integral method of Tien[4] was successfully used to predict the solidification time and the surface temperature of the cylindrical TES unit.

A dimensionless factor for heat-transfer resistance R_H^* was defined for the cylindrical geometry and the experimental resistance factors for melting and freezing were evaluated and compared with those of the theoretical bounds.

It was demonstrated that the thermal diffusivity of the PCM could be computed from the Fourier number if the time for complete solidification was available from the experiment as well as from the analytical solidification model.

Acknowledgments

The work described in this paper was supported by the Air Force Wright Aeronautical Laboratories, Wright-Patterson Air Force Base, Ohio, through the Southeastern Center for Electrical Engineering Education (SCEEE) under Contract F33615-77-C-2059. The authors are very grateful to Dr. E. Tom Mahefkey of WPAFB for initiating this work and for critically reviewing this paper.

References

[1] Wyman, C., "Thermal Energy Storage Applications: An Overview," Solar Energy Research Institute, Golden, Colo., Rept. SERI/TR-34-089, March 1979.

[2] Petri, R. J., Claar, T. D., and Tison, R. R., "High Temperature Molten Salt Thermal Energy Storage Systems," DOE/NASA/0806-79/1, NASA CR-159663, Feb. 1980.

[3] London, A. L. and Seban, R. A., "Rate of Ice Formation," *Heat Transfer Division, Transactions of ASME*, Vol. 65, Oct. 1943, pp. 771-778.

[4] Tien, R. H., "A Heat Transfer Analysis for Solidification of Rounds," *Journal of Heat Transfer, Transactions of ASME*, Vol. 102, May 1980, pp. 378-379.

[5] Goodman, T. R., "The Heat-Balance Integral and Its Application to Problems Involving a Change of Phase," *Transactions of ASME*, Vol. 80, Feb. 1958, pp. 335-342.

[6] Tao, L. C., "Generalized Numerical Solutions of Freezing a Saturated Liquid in Cylinders and Spheres," *AIChE Journal*, Vol. 13, Jan. 1967, pp. 165-169.

[7] Shamsundar, N. and Sparrow, E. M., "Analysis of Multidimensional Conduction Phase Change via the Enthalpy Model," *Journal of Heat Transfer*, Vol. 97, Sec. C., No. 3, Aug. 1975, pp. 333-340.

[8] Davison, J. E., "Evaluation of Eutectic Fluoride Thermal Energy Storage Unit Compatibility, Part I: Survey of Thermophysical Property Data and Description of Clad/Salt Sample Preparation," AFAPL-TR-92-Pt. I, Oct. 1975.

[9] Richter, R., "Thermal Energy Storage Demonstration Unit for Vuilleumier Cryogenic Cooler," AFAPL-TR-77-65, Feb. 1978.

[10] Feuermann, D. and Jacobson, D. L., "Evaluation of a Sodium Heat Pipe/Thermal Energy Storage Unit Utilizing LiF-MgF_2-KF Phase Change Material," AIAA Paper 79-1095, 1979.

[11] Bandow, H. E. and Crisp, J. N., "Analysis of Solidification in a Cylindrical Annulus with and without Internal Longitudinal Fins," School of Engineering, University of Dayton, Ohio, Rept. USDE TR 78-07, 1978.

[12] Solomon, A., "Melt Time and Heat Flux for a Simple PCM Body," *Solar Energy*, Vol. 22, No. 3, 1979, pp. 251-257.

[13] Davison, J. E., "Feasibility Study of Inorganic Oxides for Thermal Energy Storage Applications," AFAPL-TR-77-70, Nov. 1977.